Raman Spectroscopy of Isotopic Water Diffusion in Ultra-Viscous, Glassy and Gel States in Aerosol Using Optical Tweezers

James F. Davies and Kevin R. Wilson*

Chemical Sciences Division, Lawrence Berkeley National Laboratory, Berkeley, CA 94611, USA

**Correspondence to: krwilson@lbl.gov*

Abstract

The formation of ultra-viscous, glassy and amorphous gel states in aqueous aerosol following the loss of water results in non-equilibrium dynamics due to the extended timescales for diffusive mixing. Existing techniques for measuring water diffusion using isotopic exchange are limited by contact of samples with the substrate, and methods applied to infer diffusion coefficients from mass transport in levitated droplets requires analysis using complex coupled differential equations to derive diffusion coefficients. We present a new technique that combines contactless levitation using aerosol optical tweezers with isotopic exchange (D_2O/H_2O) to measure the water diffusion coefficient over a broad range (D_w ~10^{-12} – 10^{-17} m^2 s^{-1}) in viscous organic liquids (citric acid, sucrose and shikimic acid) and inorganic gels (magnesium sulfate, $MgSO_4$). For the organic liquids in binary and ternary mixtures, D_w depends on relative humidity and follows a simple compositional Vignes relationship. In $MgSO_4$ droplets, water diffusivity decreases sharply with water activity and is consistent with predictions from percolation theory. These measurements show that combing micron-sized particle levitation (a contactless measurement with rapid mixing times) with an established probe of water diffusion, D_w can be simply and directly quantified for amorphous and glassy states that are inaccessible to existing methods.

Introduction

The amount of water associated with an aqueous solution determines its physical characteristics, such as density and viscosity. On drying, the loss of water leads to discrete phase transitions such as crystallization, or continuous changes leading to the formation of highly concentrated metastable amorphous states.[1] Amorphous states can exhibit very high viscosity relative to aqueous solutions, leading to slow diffusion and altered chemical kinetics.[2–4] The formation of amorphous states is enhanced in nanometer and micron-sized aerosol due to the lack of heterogeneous surfaces that act as nucleation sites for crystallization. Fully understanding the role of aerosol in the atmosphere, for instance, requires understanding how high viscosity and slow diffusion couple with reactive gas uptake and chemical processing. However, a key challenge remains in measuring the diffusive properties and viscosity in highly concentrated aqueous solutions.

Quantifying viscosity in liquids is straightforward using bulk methods, such as a rheometry and flow-based techniques.[5,6] Aerosol particle methods have also been developed using coagulation,[2] impaction[7] or fluorescence imaging[8] to measure viscosity. The Stokes-Einstein (S-E) relationship provides a means of relating viscosity measurements to the diffusivity of solution constituents. Unfortunately, S-E has been shown to be unreliable for estimating water diffusion coefficients (D_w) in viscous media due to the ability of smaller water molecules to percolate through channels in the viscous matrix.[2,9,10]

Measurements of diffusion in highly viscous media are challenging. NMR-based methods are not applicable for slow diffusion, with lower limits in the region of ~10^{-12} m^2 s^{-1}, although rotational diffusion may be resolved to lower values.[11] Other methods using the timescales for water transport have enabled indirect estimates of water diffusion in aqueous solutions of maltose, sucrose, citric acid, magnesium sulfate and shikimic acid.[12–17] These aerosol-based methods measure the change in size and light scattering intensity during evaporation or condensation of water following changes in relative humidity (RH). These data are then analyzed by mass transport models and the best D_w is determined. A technique reported by Price and coworkers,[3,18] based on the approach of Zhu et al.,[19] uses Raman microscopy to measure radially-resolved isotopic exchange rates (at a fixed water content) for a cylinder of solution held between glass slides. By comparing the isotope concentration as a function of both position and time to predictions from a solution to Fick's

Second Law of diffusion, a single best fit value of D_w is obtained. Isotopic tracer methods have also been applied to droplets on glass cover slides.[20] Due to the relatively large sample sizes (up to a few hundred microns), measurements of isotopic exchange for low D_w (10^{-14} – 10^{-16} m^2 s^{-1}) typically require tens to hundreds of hours. Thus, maintaining stable experimental conditions (RH, temperature) over these long timescales can be challenging. In contrast, droplet measurements employ much smaller sample sizes (up to tens of microns) allowing equivalent measurements to be conducted over much shorter timescales (minutes to hours).

The isotopic tracer method of Price et al. and the mass transport method of Zobrist et al. have been applied to sucrose solutions, a common benchmark for new methods of exploring diffusion limitations.[3,12] However, there remains some disagreement between the two methods, particularly at low water content where D_w is on the order of 10^{-15} m^2 s^{-1}. Studies using parameterizations of D_w in sucrose to explain mass transport data from droplets held in optical traps have reported closer agreement to models when using the values of Zobrist.[21] This suggests that there are additional factors that must be considered or better characterized in order to relate D_w between these techniques. For instance, when concentration gradients (strictly chemical potential gradients) are present, the mutual diffusion coefficient determines the rate of mass transfer. To accurately model this process, knowledge of the solution activity of diffusing species, as well as the concentration dependence of D_w, is required. During isotopic exchange, however, the concentration gradients arise from the relative isotope concentrations, and the self-diffusion coefficient is the determining factor. Under the assumption that the diffusive properties of H_2O and D_2O are identical, a single value of D_w may be applied to understand the isotopic exchange process, simplifying the analysis and providing a more fundamental quantity describing diffusion.

In this work, we combine the benefits of single particle levitation (fast mixing timescales, contactless measurements) with an isotopic exchange technique to measure D_w. First, we measure D_w in sucrose solution droplets, benchmarking our results with established techniques. We present measurements of D_w in citric acid (CA) and shikimic acid, both explored in studies examining the role of viscosity in reactive uptake kinetics.[4,22] We discuss mixed organic particles of sucrose and citric acid, quantifying D_w as a function of mass fraction. Finally, we report new measurements of D_w in magnesium sulfate, a challenging system since crystallization prevents such measurements in macroscopic samples at low RH. In the absence of crystallization, $MgSO_4$ transitions into a two-

phase gel, resulting in slow mass transport as water diffusion only occurs through pores in the solid network of the inorganic salt.

Experimental

The work described here used a commercially available Aerosol Optical Tweezer (AOT-100 Biral) for contactless levitation of single droplets of 3 - 6 μm in radius. We modified the environmental control system to allow for rapid exchange of the gas phase humidity source between H_2O and D_2O (Figure 1) and monitored the progression of the droplet composition using Raman spectroscopy. A model using the solution to Fick's Second Law describing diffusion in a sphere was used to analyze the data by varying D_w to achieve the best fit to both the D_2O and H_2O datasets (Figure 2A). D_w are reported with an error of ±50%, reflecting the uncertainty in fits to the data, the difference between the self-diffusion coefficients of D_2O and H_2O (reported to be in the range 10 – 25%),[3] and the variability in RH (±1%). The absolute uncertainty in the RH is reported as ±2% to reflect the accuracy of the RH probes (Honeywell HIH-4602C).

Single particle confinement

In a typical optical tweezers measurement, a solution is aerosolized using an ultrasonic nebulizer and introduced into the laser trapping chamber, where a single droplet is confined and enlarged by coalescence with further droplets in the plume. The chamber is subsequently sealed and a humidified nitrogen flow is introduced to equilibrate the chamber and droplet at a known RH. A schematic of the optical tweezers arrangements is shown in Figure 1. The size and refractive index of the droplet are determined in real-time from the wavelength position of cavity enhanced resonances in the droplet, detected using Raman spectroscopy, using the proprietary Biral and University of Bristol sizing software (LARA 2.0) incorporating the algorithms of Preston and Reid.[23] Using this technique, the theoretical limits on the precision to which the radius and refractive index may be determined are, respectively, 1 nm and 0.05%. Experimentally, measurements typically have an uncertainty of ±5 nm in radius and ±0.001 in refractive index. The spontaneous Raman signals arising for the O-H stretch (at wavelength 638 – 660 nm), the C-H stretch (at wavelength 627 – 634 nm), the vinylic C=H stretch (at wavelength 634 – 637 nm) and O-D stretch (at wavelength 607 – 620 nm), are observable (see, for example, the inset of Figure 2A) and may be used to quantify the relative abundance species in the droplet.[24] For isotopic

exchange, the water supply generating the RH in the chamber was switched to D_2O, and the Raman bands corresponding to H_2O and D_2O were monitored over time (Figure 2A).

H_2O/D_2O Exchange

In order to ensure rapid exchange of the gas phase environment in the AOT chamber with D_2O vapor at a constant RH, a three-way valve system was used (Figure 1). Following cell equilibration at the measurement RH with water vapor, the gas flow was deflected away from the cell through an exhaust port, allowing a second valve to deflect the flow to a D_2O bubbler without influencing the droplet stability. The RH of the D_2O flow was allowed to stabilize at the value from the H_2O flow, after which the gas flow was redirected back into the chamber. The total time for the switch procedure is around 1-2 minutes and the chamber response time is on the order of 10's seconds. The main limitation in the response of the droplet to a change in the water isotope is the time required for the liquid deposited on surfaces within the cell to fully exchange. Until this occurs, the gas phase composition is a varying mixture of D_2O and H_2O vapor. From calibration measurements done on NaCl and LiCl solution droplets at variable humidity, the timescale for this to occur is around 20 – 60 s. It was noted for solutions that retain less water but exhibit rapid diffusive mixing in the particle phase that exchange occurs on a more rapid timescale. These calibration data allow us to estimate a limit of detection of the technique to diffusion coefficients less than approximately 10^{-13} m^2 s^{-1}.

Diffusion Theory and Raman Spectroscopy

In order to derive the water diffusion coefficient, D_w, from the timescale for isotopic exchange, a solution to Fick's Second Law of diffusion is used:[25]

$$\frac{C}{C_0} = 1 + \frac{2a}{\pi r}\sum_{n=1}^{\infty}\frac{(-1)^n}{n}\sin\frac{n\pi r}{a}\exp\left[\frac{-D_w n^2\pi^2 t}{a^2}\right]$$

where C/C_0 is the fractional concentration of D_2O in the particle during a H_2O to D_2O transition, a is the particle radius, r is the radial distance from the center of the droplet, and t is the time. For a sphere of uniform composition, this solution is used to resolve the time and positional dependence of the droplet isotopic composition during an isotopic exchange step. The model predicts that the surface region rapidly exchanges, while the time for increasing depths to exchange is much longer. Thus, a volume-averaged composition shows a sharp change initially,

corresponding to the outer layers of the particle exchanging rapidly, followed by a slower approach to complete the exchange. This was clearly observed in the experiments conducted by Price et al. where the radial composition across a liquid cylinder was measured as a function of time.[3] In the AOT, however, the spectroscopic information relates to a radially-averaged composition across the particle depth. This arises due to the laser irradiance, I_0, and beam cross-section, S, terms in the Raman intensity (N_R) as formulated by Signorell and Reid:[26]

$$N_R = \frac{\partial \sigma}{\partial \Omega}(\Delta\Omega)\frac{I_0}{h\nu}NSL$$

with Raman scattering cross-section $\partial\sigma/\partial\Omega$, solid angle $\Delta\Omega$, incident light frequency ν, molecular number concentration N, and interaction length L. In a droplet conceptually broken into radial shells of equal thickness, denoted with the index i, the focused laser beam in the AOT requires the laser irradiance incident on a shell to scale with its surface area, A_i, and the total laser power, P, thus, giving:

$$[N_R]_i \propto \frac{P}{A_i} \times N_i \times A_i \times L_i$$

The beam cross-section incident on each shell also scales with the surface area, and these terms cancel out, leading N_R to vary as a function of radial shell thickness, concentration and total laser power. Thus, each radial shell contributes to the total signal weighted by its thickness and concentration, and the scattering intensity measured experimentally corresponds to radially-averaged concentration. Accounting for this by determining a radially-averaged composition from the diffusion model leads to excellent agreement between the shape of the predicted isotope kinetics and the experimental observations. To illustrate the difference, both radial and volume averages are shown in Figure 2B. The volume averaged approach does not replicate the shape of the observed dependence for any value of diffusion coefficient, while the radial approach exhibits excellent agreement. To our knowledge, this is the first time the spontaneous Raman intensity from droplets in an optical tweezers has been used to quantify composition in particles that exhibit a gradient in the radial dimension. Previous work has assumed well mixed particles, where assumptions of radial versus volume averaging become irrelevant.

Results and Discussion

Water diffusion in binary solution droplets

The isotopic exchange method was applied to sucrose solution droplets with radii in the range 4-5 μm, and D_w as a function of RH is shown in Figure 3A. These results are compared to parameterizations reported by Price et al. and Zobrist et al., and the Stokes-Einstein predictions using the viscosity data reported by Power et al.[2,3,12] Our results are in closer agreement with the isotopic exchange measurements of Price et al. than those reported by Zobrist et al. using mass transport methods. The predictions using S-E fall many orders of magnitude below the measurements and further highlight the limitations of S-E for predicting the diffusion of small molecules in viscous media. The large difference in mobility between water and sucrose due to their molecular size contributes to the breakdown of S-E.

Measurements of water diffusion were made in CA solutions (Figure 3B) and, while D_w is larger than for sucrose at a given RH, the prediction by S-E from the viscosity data provided by Reid and coworkers[27] are in much closer agreement (although the discrepancy remains greater than an order of magnitude). Given that S-E fails to capture the behavior of water diffusion in sucrose solutions, the improved predictive power for water diffusion in CA solution may arise from the smaller difference in molecular radius between the organic and water. Water diffusion in CA was explored by Lienhard et al., at temperatures <281 K, using an optical model based on Mie theory coupled with evaporation and condensation measurements, and parameterized as a function of temperature and mole fraction of water.[13] The prediction at 293 K is shown in Figure 3B and fails to reproduce the observations reported here. The optical technique of Lienhard has also been applied to shikimic acid solution droplets by Steimer et al.[15] We observe here values of D_w which are 5 – 10 times smaller than those determined by Steimer et al. (Figure 3C), the discrepancy potentially arising from the complications associated with measuring and interpreting mutual diffusion, as discussed earlier.

A Vignes-type fit is commonly used to parameterize the relationship between composition and diffusion coefficient:

$$D_w = D_{w,w}^{0\,(\alpha x_w)} . D_{w,\mathrm{org}}^{0\,(1-\alpha x_w)}$$

where $D^0_{w,org}$, and $D^0_{w,w}$ are the diffusion coefficient of water in pure organic and in pure water, respectively. x_w is the mole fraction of water, and α is akin to an activity coefficient. Practically

any measured dependence could be well described by this relationship given the number of fit parameters usually included in α, which varies as a function of mole fraction of water and temperature. Using the water activity – mole fraction parameterization of Norrish et al.[28] (shown by Power et al.[2] to be most appropriate) for sucrose and E-AIM for CA,[29] Vignes curves were fit to the data in two ways. First, by simply assuming α = 1 and then allowing $D^0_{w,org}$ to vary, and second, using a functional form (simplified compared to that used by Lienhard et al. due to the fixed temperature of these measurements) of α given by:

$$\ln(\alpha) = A(1 - x_w)^3$$

and allowing the constant, A, and $D^0_{w,org}$ to vary. These fits are shown in Figure 3A and 3B and both yield a reasonable description of the data, with the $\alpha(x_w)$ method, as expected given the additional fit parameters, performing better.

Water diffusion in ternary solutions

To probe the applicability of the simple Vignes formulation in more complex systems, mixtures of CA and sucrose were investigated in 3:1, 2:1 and 1:1 molar ratios (Figure 4). It is apparent that D_w scales between the limitation cases of the binary solution of citric acid and sucrose, and by plotting the dependence of $\log(D_w)$ with mass fraction, a linear relationship is clearly observed at a given RH (Figure X). Thus, the values of $\log(D^0_{w,CA})$ and $\log(D^0_{w,suc})$ established from the binary solutions were scaled linearly using the mass fraction. In order to estimate the mole fraction of water in the ternary solutions, the Zdanovskii-Stokes-Robinson relationship was applied using the dependence of x_w on RH in the binary solutions. Using these data, the Vignes equation was used to estimate the diffusion coefficient for the mixtures, using α = 1. There is close agreement between data and prediction despite the simplicity of the relationship and assumptions of ideality. It may be the case that the opposing non-ideality effects in the limiting cases of the binary solutions cancel out in the ternary system. Thus, one might expect complex mixtures to exhibit a relatively simple dependence of D_w on composition and, for application in atmospheric modelling, such a simple dependence is desirable.

Gel formation in inorganic solutions

While ultra-viscous and glassy states are encountered with some organic solutions, inorganic salts typically crystallize at low RH forming distinct solid phases (i.e. efflorescence). An alternative to

this process is the formation of a micro-gel – a two phase amorphous state where saturated aqueous solution and a solid network coexist. Magnesium sulfate is one example of a gel forming salt, as the divalent ions allow an inorganic network to develop. Water transport becomes limited by slow percolation through pores in the network. In macroscopic bulk samples, efflorescence or localized gel formation readily occurs, making measurements of water diffusion challenging. However, in a contactless technique, the gel phase forms readily, and water transport limitations can be observed.[20,30]

The dependence of D_w on RH in $MgSO_4$ solution droplets was measured, as shown in Figure 5. These data exhibit a much stronger decrease in D_w as a function of RH than the organic systems. While data at higher RH is not accessible to this technique, Price et al. report values down to an RH of 60%, and combined with our data suggest a rapid onset of diffusion limitations at an RH in the range 30 – 45%, consistent with a previously reported range of 30 – 55%. A recent study by Leng et al.[14] report values of D_w at 30%, 20% and 0% using a pulsed RH technique on droplets deposited on cover slides. At 30%, there is excellent agreement with our data. At lower RH's we observe diffusion to be slower (by a factor of ~5x). This may be a consequence of radial inhomogeneity in droplets during the pulsed RH procedure, leading to measurements that report an average value of D_w for a droplet with large compositional gradients. The AOT data we report corresponds to fully equilibrated particles at the measurement RH, and so provides a measurement of D_w for a sample of uniform composition.

The form of the dependence of D_w on RH during gel formation closely resembles predicted behavior from percolation theory for a mixed system with two different diffusion coefficients[31,32]. Percolation theory treats a system as packed hard spheres (the pores) in a matrix (the solid), with two limiting diffusion coefficients describing water transport in the solid inorganic matrix, D_s, and the liquid pores, D_p. The overall D_w is predicted to be:[31]

$$D_w = \left[D'_p + D'_s + \left\{ \left(D'_p + D'_s \right)^2 + 2(Z-2) D_p D_s \right\}^{\frac{1}{2}} \right] \Big/ (Z-2)$$

$$D'_p = D_p \left(\frac{Z V_p}{2f} - 1 \right)$$

$$D_s' = D_s\left(\frac{Z}{2}\left\{1-\frac{V_p}{f}\right\}-1\right)$$

where Z is the coordination number, f is the packing fraction, and V_p is the volume fraction of the pores. By extrapolating the hygroscopicity data of Ha et al. to 0% RH,[33] it was determined that the gel phase consists of $MgSO_4 \cdot 3H_2O$. For RH > 0, the solid phase and a saturated aqueous phase coexist. Thus, not all of the $MgSO_4$ is bound in the solid phase. To account for this, D_p was taken from the slowest aqueous diffusion constant measured by Price et al. prior to gel formation (2×10^{-11} m^2 s^{-1}). The mole fraction of $MgSO_4$ in the liquid in the pores was assumed to be 0.067; the saturation concentration of $MgSO_4$ in water. V_p was estimated from the hygroscopicity data, while f and Z were allowed to vary to best replicate the data. The best approximation of the data to percolation theory is shown in Figure 5 using f = 0.85 and Z = 4. The model exhibits a strong dependence on these parameters (Figure 5B) and, while their physical interpretation in the $MgSO_4$ gel is somewhat unclear, the distinct functional form of D_w vs. RH is reproduced by the theory. By applying the concepts of percolation theory, the onset of gel formation and the sharp fall in D_w may be ascribed to the development of the solid portion of the gel throughout the whole droplet. This leads to a state where aqueous channels through the droplet become diminishingly small and diffusion through the solid phase becomes the limiting step.

Conclusions

In summary, we highlight the unique advantages of the droplet-based isotopic tracer method for measurements of diffusion coefficients. Firstly, the simplicity of the system allows values of D_w to be determined with very little computation, eliminating assumptions relating to concentration and viscosity gradients. Secondly, compared to the liquid disc method of Price et al., the timescales for equilibration are much shorter, allowing access to measurements of D_w down to ~10^{-17} m^2 s^{-1} in a single day, which would otherwise take weeks. Thirdly, by eliminating any surfaces, samples that exhibit contact efflorescence may be studied, having significant advantages for atmospheric samples, which routinely exist in highly supersaturated states. We have demonstrated excellent agreement to previous methods of measuring diffusion via isotopic exchange and have shown the applicability of a simple Vignes relationship for complex mixtures. However, we observe a significant discrepancy between diffusion measurements made using mass transport and those made using isotopic exchange. Such observations may reveal complexities associated with

modelling mass transport in viscous aerosol that have not yet been fully resolved. The resolution of gel formation in magnesium sulfate highlights the potential utility of the technique in identifying phase behavior that leads to abrupt changes in water mobility (e.g. hydrophobic phase separation). Further applications of this technique will explore the changing role of water diffusion during chemical transformation, providing valuable insight into the influence of oxidative aging in determining diffusive properties of atmospheric aerosol, and the role of diffusion in regulating the rate of chemical change.

Acknowledgements

This work is supported by the Department of Energy's Office of Science Early Career Research Program and by the Director, Office of Energy Research, Office of Basic Energy Sciences, Chemical Sciences, Geosciences, and Biosciences Division of the U.S. Department of Energy under Contract No. DE-AC02-05CH11231.

References

(1) Krieger, U. K.; Marcolli, C.; Reid, J. P. *Chem. Soc. Rev.* **2012**, *41*, 6631–6662.

(2) Power, R.; Simpson, S.; Reid, J.; Hudson, A. *Chem. Sci.* **2013**, *4*, 2597–2604.

(3) Price, H. C.; Murray, B. J.; Mattsson, J.; O'Sullivan, D.; Wilson, T. W.; Baustian, K. J.; Benning, L. G. *Atmos. Chem. Phys.* **2014**, *14*, 3817–3830.

(4) Davies, J. F.; Wilson, K. R. *Chem. Sci.* **2015**, *6*, 7020–7027.

(5) Booth, A. M.; Murphy, B.; Riipinen, I. A.; Percival, C. J.; Topping, D. O. *Env. Sci. Technol.* **2014**, *48*, 9298−9305.

(6) Grayson, J. W.; Song, M.; Sellier, M.; Bertram, A. K. *Atmos. Meas. Tech.* **2015**, *8*, 2463–2472.

(7) Virtanen, A.; Joutsensaari, J.; Koop, T.; Kannosto, J.; Yli-Pirila, P.; Leskinen, J.; Makela, J. M.; Holopainen, J. K.; Poschl, U.; Kulmala, M.; Worsnop, D. R.; Laaksonen, A. *Nature* **2010**, *467*, 824–827.

(8) Hosny, N. A.; Fitzgerald, C.; Tong, C.; Kalberer, M.; Kuimova, M. K.; Pope, F. D. *Faraday Discuss.* **2013**, *165*, 343–356.

(9) Kumar, S. K.; Szamel, G.; Douglas, J. F. *J. Chem. Phys.* **2006**, *124*, 214501.

(10) Molinero, V.; Goddard, W. A. *Phys. Rev. Lett.* **2005**, *95*, 1–4.

(11) Martin, D. R.; Ablett, S.; Darke, a; Sutton, R. L.; Sahagian, M. *J. Food. Sci.* **1999**, *64*, 46–49.

(12) Zobrist, B.; Soonsin, V.; Luo, B. P.; Krieger, U. K.; Marcolli, C.; Peter, T.; Koop, T. *Phys. Chem. Chem. Phys.* **2011**, *13*, 3514–3526.

(13) Lienhard, D. M.; Huisman, A. J.; Bones, D. L.; Te, Y.-F.; Luo, B. P.; Krieger, U. K.; Reid, J. P. *Phys. Chem. Chem. Phys.* **2014**, *16*, 16677–16683.

(14) Leng, C.-B.; Pang, S.-F.; Zhang, Y.; Cai, C.; Liu, Y.; Zhang, Y.-H. *Env. Sci. Technol.* **2015**, *49*, 9107–9115.

(15) Steimer, S. S.; Krieger, U. K.; Te, Y.-F.; Lienhard, D. M.; Huisman, a. J.; Luo, B. P.; Ammann, M.; Peter, T. *Atmos. Meas. Tech.* **2015**, *8*, 2397–2408.

(16) Parker, R.; Ring, S. G. *Carbohyd Res.* **1995**, *273*, 147–155.

(17) Cai, C.; Tan, S.-H.; Chen, H.-N.; Ma, J.-B.; Wang, Y.; Reid, J. P.; Zhang, Y. H. *Phys. Chem. Chem. Phys.* **2015**, *17*, 29753–29763.

(18) Price, H. C.; Mattsson, J.; Zhang, Y.; Bertram, A.; Davies, J. F.; Grayson, J. W.; Martin, S. T.; O'Sullivan, D.; Reid, J. P.; Rickards, A. M.; Murray, B. J. *Chem. Sci.* **2015**, *6*, 4876–4883.

(19) Zhu, L.; Cai, T.; Huang, J.; Stringfellow, T. C.; Wall, M.; Yu, L. *J. Phys. Chem. B* **2011**, *115*, 5849–5855.

(20) Li, K.-K.; Wang, F.; Zeng, G.; Reid, J. P.; Zhang, Y.-H. *J. Phys. Chem. B* **2011**, *115*, 14397–14403.

(21) Rickards, A. M. J.; Song, Y.-C.; Miles, R. E. H.; Preston, T. C.; Reid, J. P. *Phys. Chem. Chem. Phys.* **2015**, *17*, 10059–10073.

(22) Steimer, S. S.; Lampimäki, M.; Coz, E.; Grzinic, G.; Ammann, M. *Atmos. Chem. Phys.* **2014**, *14*, 10761–10772.

(23) Preston, T. C.; Reid, J. P. *J. Opt. Soc. Am. A* **2013**, *30*, 2113–2122.

(24) Dennis-Smither, B. J.; Marshall, F. H.; Miles, R. E. H.; Preston, T. C.; Reid, J. P. *J. Phys. Chem. A* **2014**, *118*, 5680–5691.

(25) Seinfeld, J. H.; Pandis, S. N. *Atmospheric Chemistry and Physics: From Air Pollution to Climate Change*; Wiley, 1998.

(26) Kwamena, N.-O. A.; Reid, J. P. In *Fundamentals and Applications in Aerosol*

Spectroscopy; Signorell, R., Reid, J. P., Eds.; CRC Press, 2011.

(27) Marshall, F. H.; Miles, R. E. H.; Song, Y.-C.; Ohm, P. B.; Reid, J. P.; Dutcher, C. S. *Pers. Commun. Manuscr. Submitt.*

(28) Norrish, R. S. *J. Food Technol.* **1966**, *1*, 25–39.

(29) Peng, C.; Chow, A. H. L.; Chan, C. K. *Aerosol Sci. Technol.* **2001**, *35*, 753–758.

(30) Davies, J. F.; Haddrell, A. E.; Miles, R. E. H.; Bull, C. R.; Reid, J. P. *J. Phys. Chem. A* **2012**, *116*, 10987–10998.

(31) Murata, T.; Lee, M. S.; Tanioka, A. *J. Colloid Interface Sci.* **1999**, *220*, 250–254.

(32) Shiraiwa, M.; Ammann, M.; Koop, T.; Pöschl, U. *Proc. Natl. Acad. Sci.* **2011**, *108* (27), 11003–11008.

(33) Ha, Z.; Chan, C. K. *Aerosol Sci. Technol.* **1999**, *31*, 154–169.

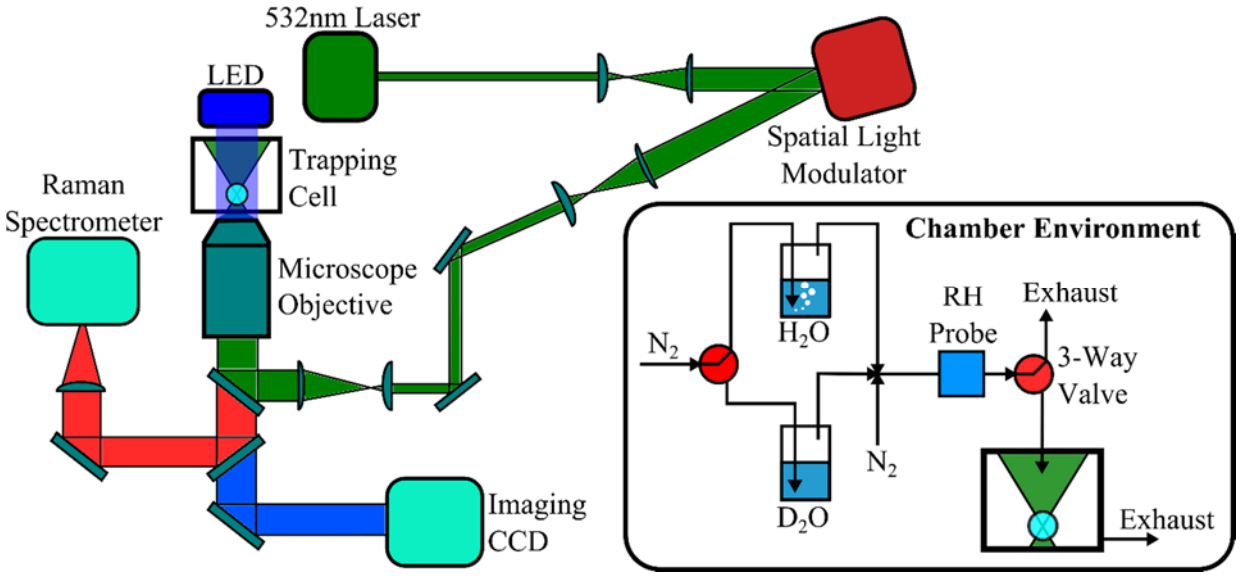

386

387 **Figure 1:** Standard optical tweezers (Biral AOT 100) arrangement and (inset) the valve system
388 used to initiate the exchange between D_2O and H_2O.

389

390

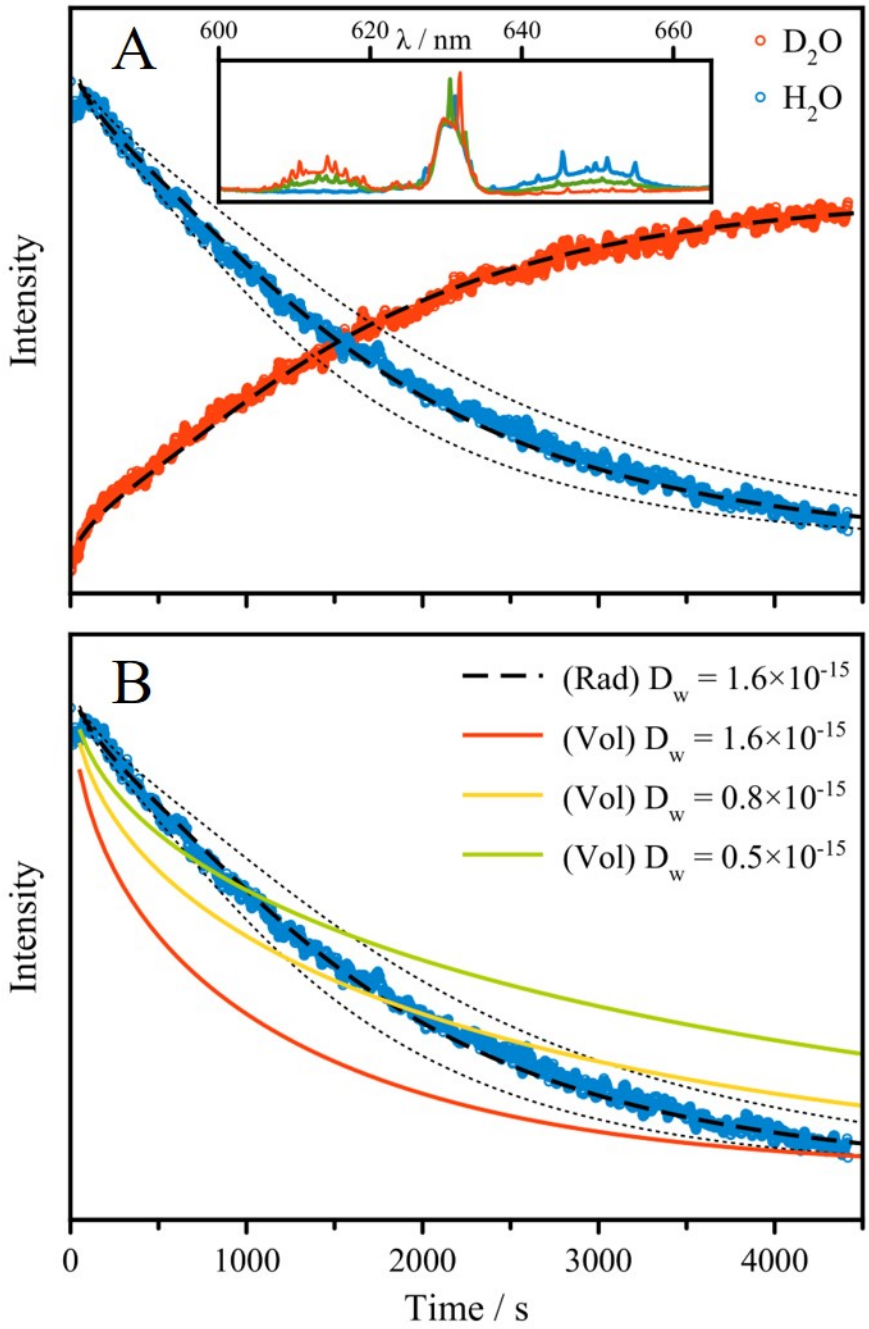

Figure 2: (A) Raman band intensity corresponding to H_2O and D_2O stretching vibrations during isotopic exchange in a 4.8 µm sucrose droplet at 32% RH. Black dash lines indicate model with D = 1.6×10^{-15} m^2 s^{-1} with a ±20% variation indicated by the dashed lines. (Inset) Full Raman spectrum prior to (blue), during (green) and after (red) the exchange. (B) Radially-averaged composition (dashed lines) and volume-averaged composition (solid lines) simulations for a sucrose droplet at 32% RH. Diffusion coefficients are indicated in m^2 s^{-1}. The dotted lines represents a ±20% uncertainty in D_w used in the simulation for the radially-averaged case.

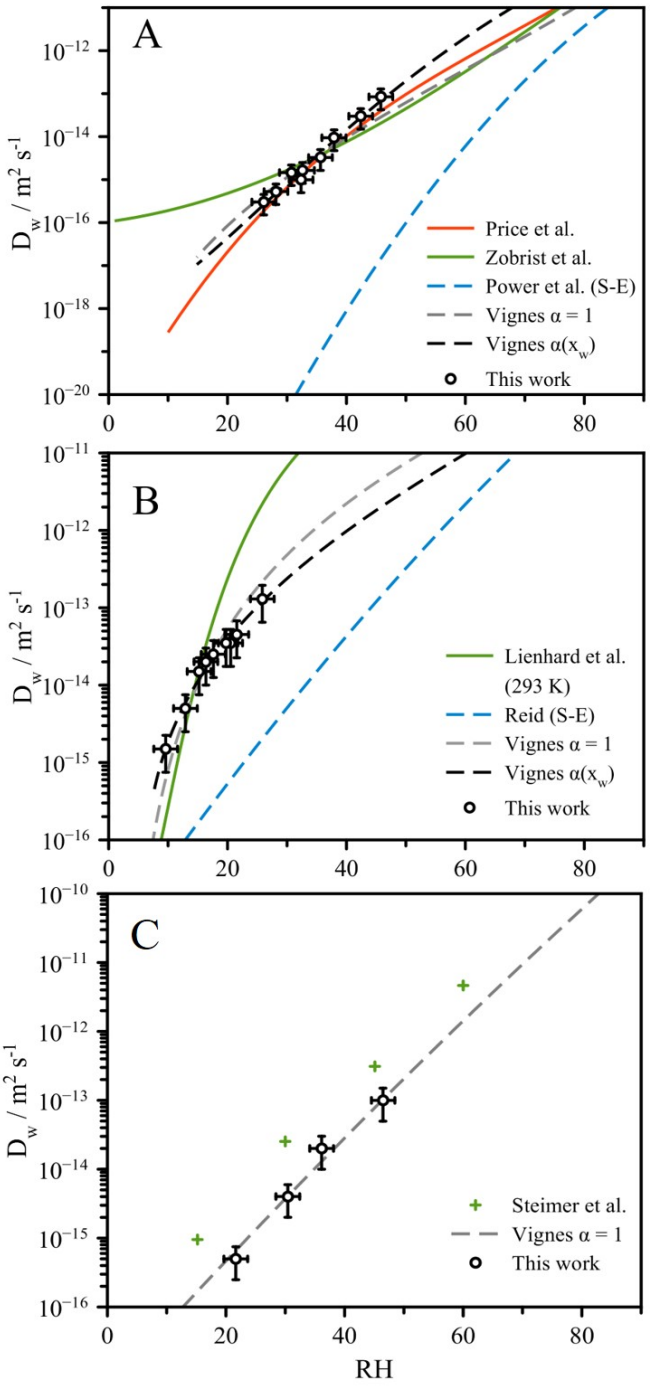

Figure 3: (A) D_w as a function of RH for sucrose droplets compared to diffusion measurements derived from mass transport (Zobrist et al.[12]), isotopic exchange on a cover slide (Price et al.[3]), and estimates using Stokes-Einstein viscosity (Power et al.[2]). The Vignes fits are shown for $\alpha = 1$ and $\alpha(x_w)$ as described in the text. (B) D_w as a function of RH for CA droplets compared to the mass transport / optical approach of Lienhard,[13] and estimates using the S-E prediction on the viscosity data of Reid and coworkers.[27] Vignes fits shown as described in (A). (C) D_w in shikimic acid as a function of RH compared to the data reported by Steimer et al. using the mass

transport/optical approach of Lienhard.[13,15] The Vignes fit uses the thermodynamic data of Steimer et al. and $\alpha = 1$ is assumed.

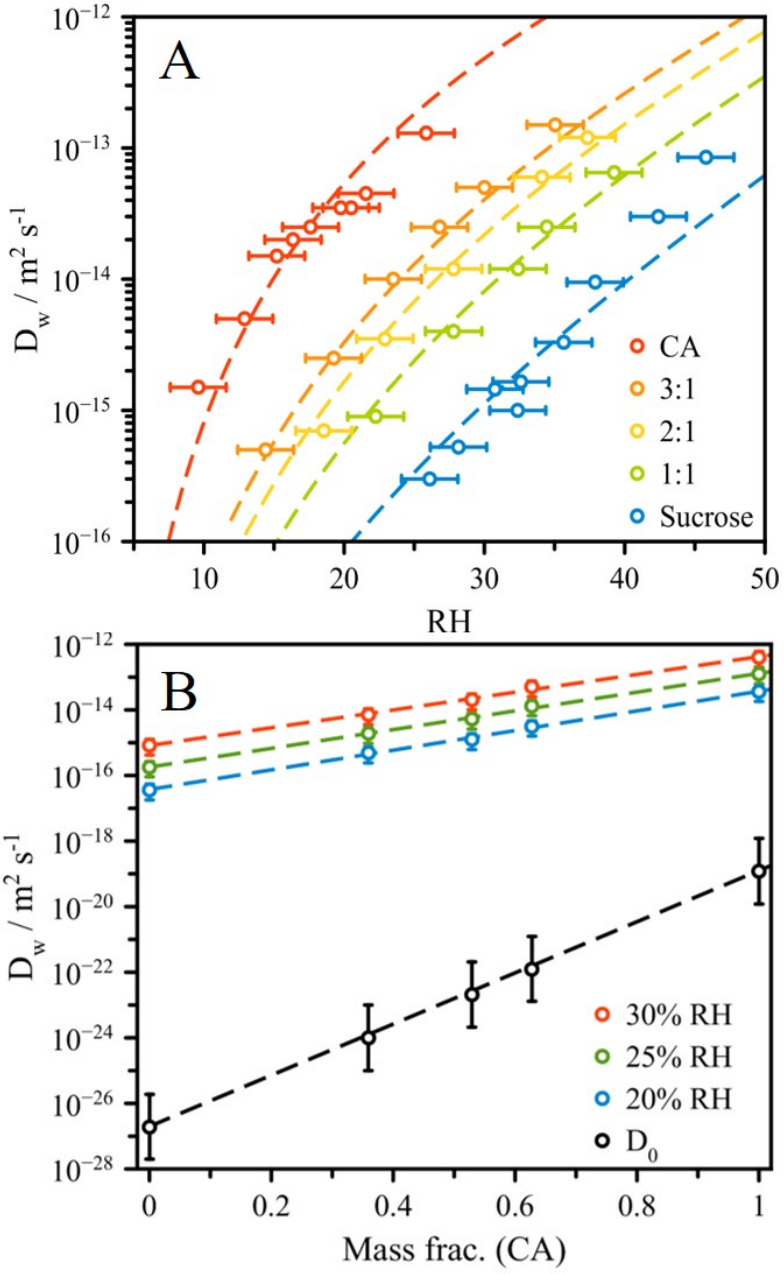

Figure 4: (A) D_w for molar ratio mixtures of citric acid and sucrose as a function of RH. The Vignes predictions with $\alpha = 1$ and assuming a linear relationship for $\log(D^0_{w,mix})$ with mass fraction of CA. (B) Water diffusion coefficient in mixtures of CA and sucrose at the specified RH. D_w vs RH curves were interpolated to infer a value of D_w at the same RH for each dataset. Colored dash lines represent linear fits. Black dash line represents a linear fit between the values of $\log(D_0)$ for pure CA and sucrose determined from the Vignes fits with $\alpha = 1$, while the black points represent D_0 fit separately for each dataset, using individual Vignes fits (with $\alpha = 1$) for each mixture. The uncertainty in D_0 is an order of magnitude.

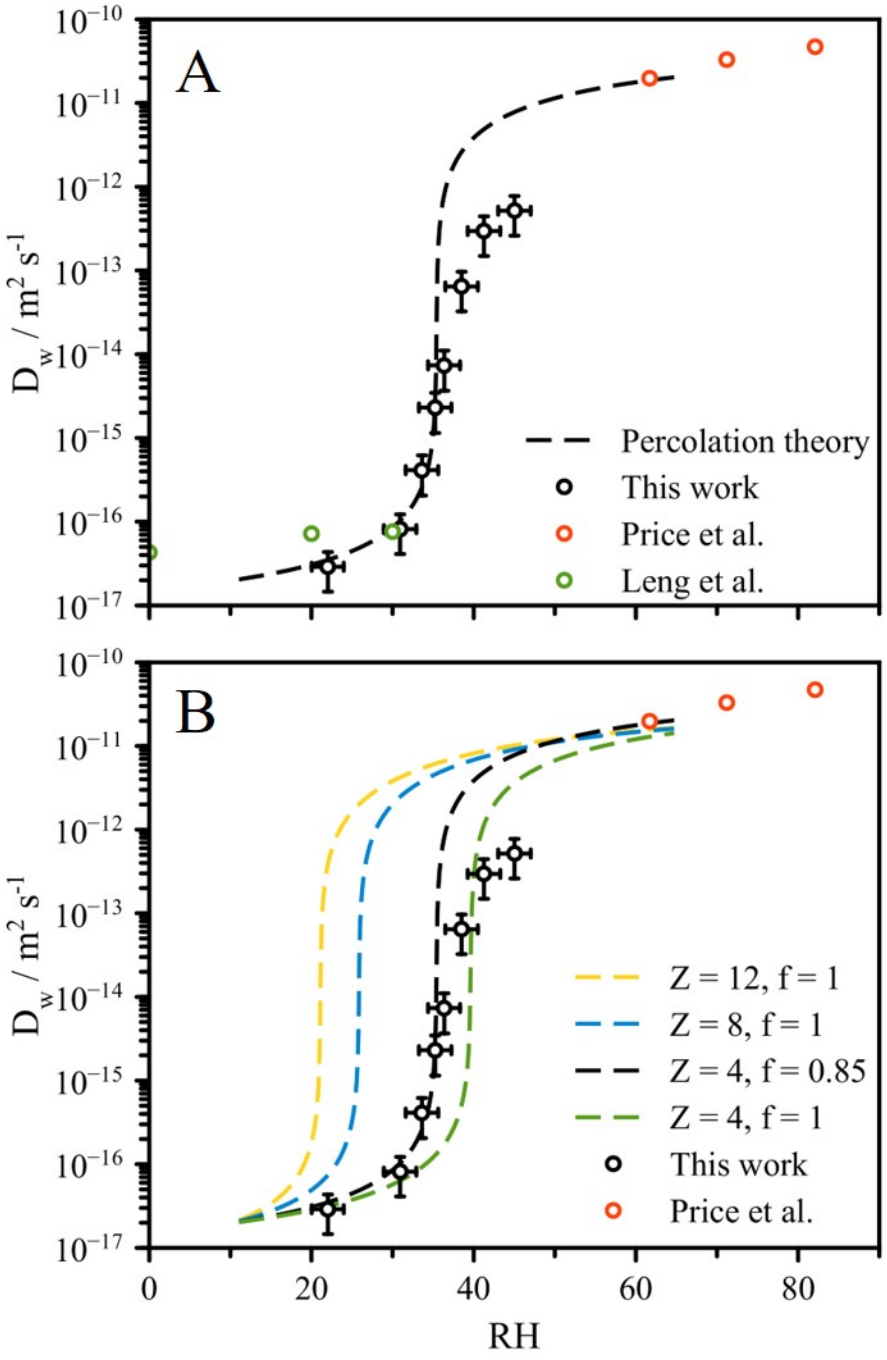

423

424 **Figure 5:** (A) D_w as a function of RH for magnesium sulfate. Gel formation is indicated by the
425 rapid decrease of D_w, as predicted by percolation theory (as described in the text and SI). The
426 isotopic exchange values of Price et al.[3] and those determined using the pulsed RH method of Leng
427 et al.[14] are also shown. (B) A comparison of the percolation theory predictions for a range of values
428 of coordination number (Z) and packing fraction (f).

429